

THE EFFECT OF STRUCTURE DEFECTS ON THE FATIGUE BEHAVIOUR OF AZ91 MAGNESIUM ALLOY PREPARED BY SAND CASTING AND SQUEEZE CASTING

FRANTIŠEK HNILICA^{1*}, VLADIVOJ OČENÁŠEK², IVANA STULÍKOVÁ³,
BOHUMIL SMOLA³

¹UJP PRAHA, a.s., Nad Kamínkou 1345, 156 10 Prague 5, Czech Republic

²Research Institute for Metals, Ltd., Panenské Břežany 50, 250 70 Odolena Voda, Czech Republic

³Faculty of Mathematics and Physics, Charles University, Ke Karlovu 5, 121 16 Prague 2, Czech Republic

Received 3 December 2004, accepted 30 March 2005

The microstructure, tensile and fatigue properties of the magnesium alloy AZ91 prepared by two different casting methods, i.e. by conventional sand casting and squeeze casting, were studied. In addition, the morphology of fracture surface of fatigue specimens was examined. The mechanisms of crack initiation and growth were studied, too. Correlations between the occurrence of structure defects and the deterioration of alloy properties were looked for. The tensile and fatigue properties of the squeeze-cast samples were found to be better than those of the sand-cast samples. The former samples possess a finer grain structure and, in contrast to the latter, rarely contain tiny pores. The mean fatigue life for 50% probability to failure of the sand-cast alloy is of 3.3×10^5 cycles at maximum stress of 90 MPa and 3.9×10^4 cycles at maximum stress of 100 MPa. The squeeze-cast alloy exhibits fatigue life of 3.3×10^5 cycles at the higher load, i.e. 100 MPa. The number of fatigue cycles to fracture is affected appreciably by structure defects, i.e. by the presence of pores in the sand-cast material and of inclusions, oxide film and phase clusters in the material prepared by squeeze casting.

Key words: magnesium alloy, fatigue properties, structure, sand casting, squeeze casting, fracture morphology, structure defects

*corresponding author, e-mail: hnilica@ujp.cz

1. Introduction

Magnesium alloys are at present subject of extensive investigation. In addition to aluminium alloys, magnesium alloys can be employed with a view to achieving appreciable weight reduction of vehicles, cars in particular [1, 2, 3]. Efforts are made to benefit from the assets of Mg alloys, especially from their favourable density-strength ratio. Furthermore, shortcomings such as low stability at high temperatures [4], low plasticity [5, 6], and poor fatigue properties [8, 9], that were the limiting factors for the wider application of these alloys, are nowadays overcome for most part. Currently, cast alloys are predominantly used. In parallel to the development of novel types of alloys based on the optimization of chemical composition by additional elements alloying and of the associated heat treatment and based on investigations of their precipitation behaviour, new casting technology processes, such as the squeeze casting method, are being developed [10, 11]. The aim of the experiments reported here was to compare the structure and fatigue properties of AZ91 samples obtained by sand and squeeze casting, respectively.

2. Experimental

Specimens of the AZ91 magnesium alloy 90 mm × 70 mm × 200 mm and 100 mm × 100 mm × 67 mm in size were prepared by sand and squeeze casting, respectively. The chemical composition of the two materials is given in Table 1. The squeeze casting process was conducted at temperature of 800 °C under Ar + 1 % SF₆ protective atmosphere applying a two-stage pressure regime of 50 MPa and 150 MPa.

Table 1. Composition of the experimental alloys [mass %]

	Al	Zn	Mn	Cu	Si	Fe	Ni
Sand-cast	9.14	0.78	0.23	0.0085	0.024	0.0044	0.0029
Squeeze-cast	9.21	0.71	0.20	0.0032	<0.002	0.0058	0.0036

No additional heat treatment was applied. Samples were taken from the castings for structure analysis by light microscopy and for tensile and fatigue tests. Fatigue tests were performed on smooth circular specimens with bodies 7 mm in diameter, with M 16 × 1 threaded heads. The test specimens were stressed in an asymmetric cycle with $R = 0$ on a Testronic 8601 high-frequency pulsator at 85–90 Hz. The test was ultimately completed by fracture. One stress level was chosen and at least 6 test specimens were tested at this level. The samples for fatigue tests as well as for tensile tests were taken from different positions along the cross section of the castings so as to describe the inhomogeneity of the material.

The fracture surfaces were examined on a JEOL JSM 5510 LV scanning electron microscope and by light microscopy on metallographic samples oriented perpendicularly to the fracture plane in the direction of propagation of the fatigue crack. In addition to the qualitative assessment of fatigue crack initiation and propagation mechanisms, the length of fatigue cracks l_u was measured in the radial direction from the initiation point and the total area of fatigue crack projection A_u was determined. The area of the projection of initiation defects A_{def} was also evaluated and their location in the interior or at the surface of test specimens was determined. Defects at the place of crack initiation are regarded as initiation defects. As proposed in [12], the initiation sites were sorted into two groups with respect to their distance from specimen surface: surface and internal defects. The mean diameter of the equivalent circles corresponding to the projected sections A_{def} of initiation defects was chosen as the critical distance for this classification. Defects at distances larger than this value were regarded as internal defects, whereas defects at distances smaller than this value and defects adjacent to the surface were held as external (surface) defects. The stress intensity factor was also determined as a parameter, which is useful in the assessment of the effect of defects involved in the initiation of fatigue cracks. For this purpose, the procedure suggested in [13] was employed. The $K_{\text{max,in}}$ value was calculated as

$$K_{\text{max,in}} = \sigma_{\text{max}} \sqrt{\pi \alpha \sqrt{A_{\text{def}}}}, \quad (1)$$

where σ_{max} is maximum stress, $\alpha = 0.65$ for surface defects and $\alpha = 0.5$ for internal defects. The quantitative evaluation was performed on a Laboratory Imaging LUCIA DI image analyser.

3. Results and discussion

3.1 Structure and mechanical properties

The structure of both materials is shown in Fig. 1 and Fig. 2, respectively. Both samples exhibit cast structure typical of the AZ91 alloy. Due to the low cooling rate, the $\text{Mg}_{17}\text{Al}_{12}$ β -phase occurs both in the form of massive well-confined formations along dendrite boundaries and in the form of fine lamellas discontinuously precipitated in the surroundings of the massive form. The grains are finer in the squeeze-cast samples than in the sand-cast samples. The mean size of the dendrite cells is $400 \mu\text{m}$ and $125 \mu\text{m}$ in sand and squeeze cast materials, respectively. The different cooling conditions resulted in a smaller size of both the primarily formed and the precipitated β phase in the material obtained by squeeze casting as compared to the sand casting process. In addition to the β phase, the structure involves tiny elongated particles of the Mg_2Si phase (in the material obtained by

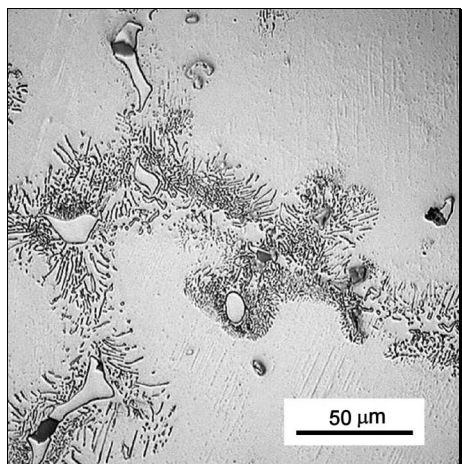


Fig. 1. Structure of sand-cast AZ91 alloy.

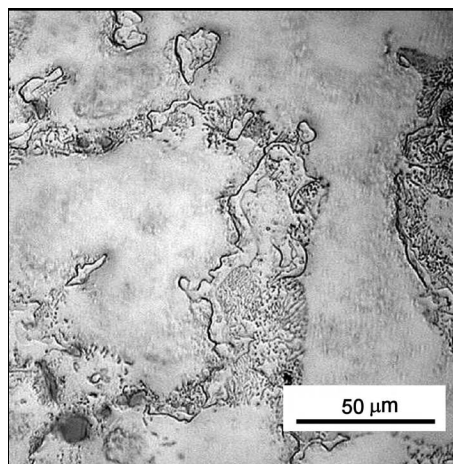


Fig. 2. Structure of squeeze-cast AZ91 alloy.

sand casting only) and of a Al-Mn type phase. Pores were present in the material obtained by sand casting, whereas in the structure of the material obtained by squeeze casting, pores occurred rarely. The latter material, however, contained structure defects of the type of phase clusters, oxide film and large inclusions.

3.2 Mechanical properties

The tensile properties (R_m , $R_{p0.2}$ and A) of both cast materials are given in Table 2. The material obtained by squeeze casting exhibits higher R_m and $R_{p0.2}$ than the material obtained by sand casting, although both parameters exhibit an appreciable scatter in both types of casting. This concerns especially strength. For $R_{p0.2}$ and A , the scatter is smaller for the samples obtained by squeeze casting than for the samples obtained by sand casting.

Table 2. Mechanical properties of experimental AZ91 alloy samples

	Sand-cast			Squeeze-cast		
	R_m [MPa]	$R_{p0.2}$ [MPa]	A [%]	R_m [MPa]	$R_{p0.2}$ [MPa]	A [%]
Mean	129	85.5	3.2	Mean	169	99.1
St. dev.	42	15.0	1.4	St. dev.	13.9	0.8

3.3 Fatigue tests

The sand-cast material was tested at stress levels of $\sigma_{\max} = 90$ MPa and 100 MPa at $R = 0$. The fatigue lives were plotted in log-normal probability scale. The results, along with the fatigue lives of the material obtained by squeeze casting, are shown in Fig. 3. It is evident that the distribution of the fatigue lives of the former material at both stress levels contains two peaks, i.e. the lives fall into two groups. A similar division of the samples into two groups was observed also in the case of mechanical properties R_m and $R_p0.2$ [12].

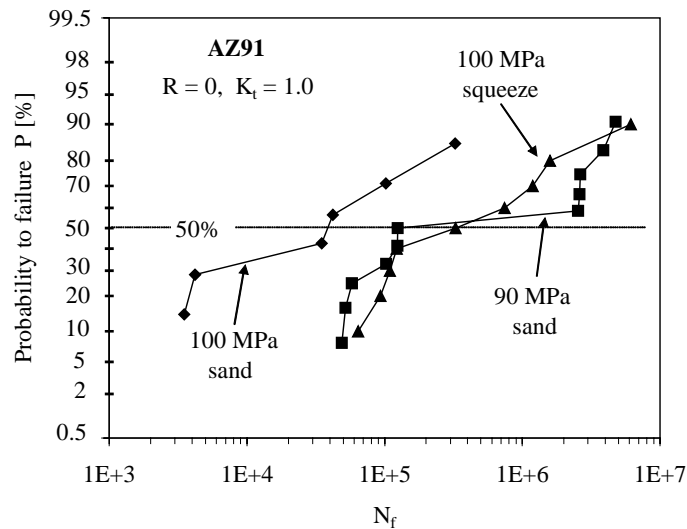


Fig. 3. Fatigue life distribution curves for sand cast and squeeze cast AZ91 alloy.

Tentative tests at 90 MPa of the material obtained by squeeze casting indicated that the lifetime of this material will be substantially longer than that of the sand-cast material (over 10^6 cycles). For this reason, in the case of the squeeze cast material, only the higher load level, $\sigma_{\max} = 100$ MPa, was checked. The fatigue lives of the squeeze-cast samples do not belong to two separate groups differing by their magnitude, contrarily to the sand cast materials. On the other hand, the scatter of fatigue lives of both materials is comparable. The mean lifetime for probability to failure $P = 50\%$ is of 3.3×10^5 cycles and it is the same for both the sand cast material tested at 90 MPa and squeeze cast material tested at stress level of 100 MPa. The fatigue resistance of the squeeze cast material is definitely better than this of the sand cast material, which mean fatigue life at stress level

$\sigma_{\max} = 100$ MPa is of only 3.9×10^4 cycles. However, when interpreting fatigue test results, structure inhomogeneity should be taken into account. The inhomogeneity is due to defects present in the castings, particularly in the sand-cast material.

3.4 Fractography

a) AZ91 samples prepared by sand casting

It was observed that fatigue cracks initiate invariably from pores, especially from surface pores (by the above criteria) in all cases but two. An example illustrating typical initiation defects is shown in Fig. 4. From the qualitative aspect, the mechanisms of fatigue crack growth and fast final fracture were identical in all samples. Therefore a summary description is given here. With respect to the typical morphological patterns, four regions can be distinguished on the fracture surface. In Fig. 5, the regions are labelled A, B, C, and final fracture surface D. The regions are also shown at the fracture line of the main crack, i.e. in the picture showing the perpendicular section through the fracture surface oriented in the direction of its fatigue propagation (Fig. 6). In the bottom part of the figure, under the fracture line, a latent crack is also shown. The latent crack stopped after nucleation and initial propagation. The shapes of the fracture line and latent crack give an idea

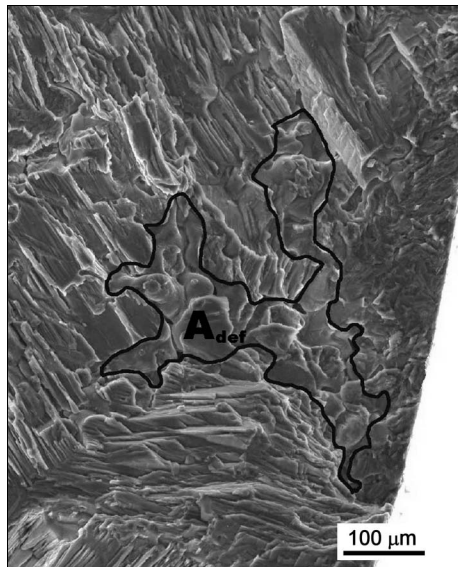


Fig. 4. Example of pore that acted as fatigue crack initiation site. Initiation defect area is labelled A_{def} .

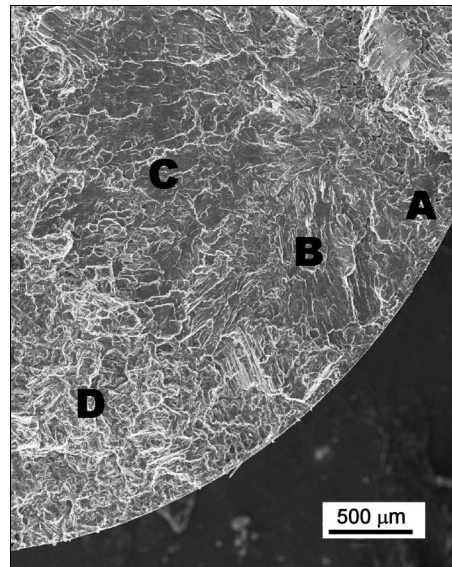


Fig. 5. Fracture surface indicating different regions inspected with SEM.

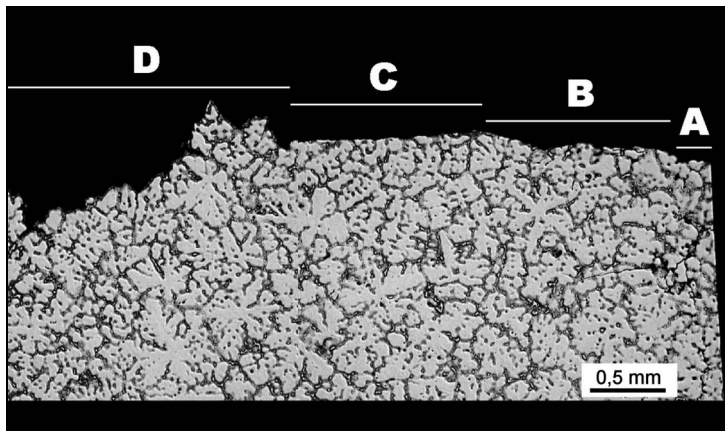


Fig. 6. Perpendicular section through fracture oriented in direction of fatigue crack propagation. Different regions are labelled. In bottom part of figure, latent crack is also shown.

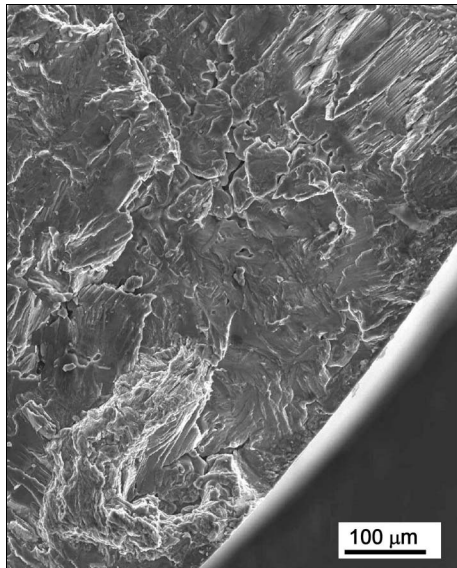


Fig. 7. Region labelled A with relatively flat fracture surface.

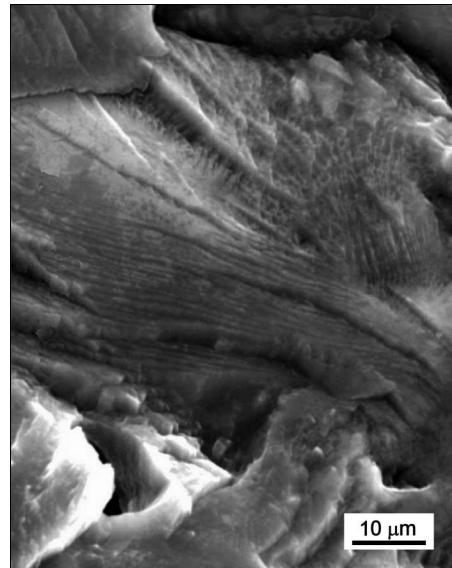


Fig. 8. Detail view on region A. Facet with parallel steps and shallow dimples.

about the relationship between the material structure and the crack initiation and propagation mechanisms.

The region A exhibits a relatively smooth, only slightly corrugated fracture surface. This region is only found in some cases at proximity of small pores at fatigue crack initiation sites (Fig. 7). A detailed view at high magnification shows that this region of the fracture surface is formed by a number of tiny facets with different orientation of basically parallel steps or “ridges” (Fig. 8). Some facets display hints of tiny, very shallow dimples (Fig. 8). The occurrence of region A is apparently affected by the presence of pores. This region is absent in samples with pores of large size. Large pores acting as initiation sites are directly associated with fracture region of type B.

The adjacent fracture surface region, i.e. region B, is characterized by larger facets with parallel or complex serrations (or steps) (serrated facets) (Fig. 9) or by larger facets with river-like patterns (Fig. 10). The detailed appearance and orientation of the serrations with respect to the macroscopic fatigue crack propagation direction vary,

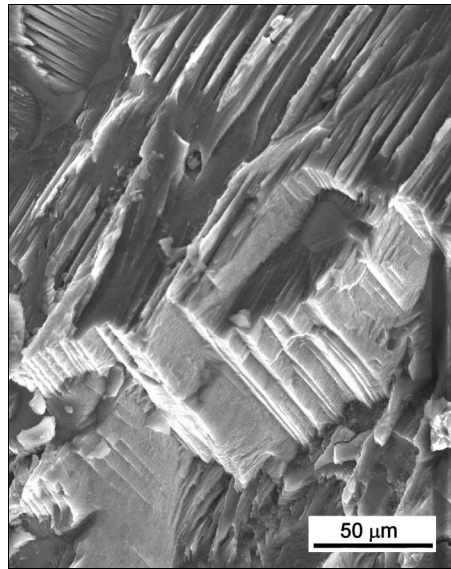


Fig. 9. Fatigue fracture facet with serrations and steps morphology (region B).

apparently in dependence on the crystallographic orientation of the individual failed dendritic cells. In this region, the fracture is predominantly transcrystalline and at the beginning, the direction of crack growth can divert occasionally from the direction perpendicular to the principal stress axis (Fig. 6). Merely in positions where the interdendritic zone is weakened by the presence of small pores (Fig. 6), the fracture passes through such a zone. The crack then can be branched, and rather extensive secondary cracks can form.

Starting approximately at fatigue crack length $l = 1.5$ mm for the stress level 90 MPa and $l = 1.3$ mm for the stress level 100 MPa, the mechanism of fracture is altered (region C in Fig. 5). The morphological features on the fracture facets, characterized by a system of clear-cut serrations or steps, change entirely their microfractographic patterns (Fig. 11). The light lines in the figures show the microscopic steps separating the fatigue microareas (patches). The shape of the patches is complex, with a predominant orientation in the direction of local propagation of the fatigue crack. As in the preceding region B, the fatigue crack propagation is transcrystalline. The detailed patterns on the fatigue patches, however, still demonstrate the effect of the crystallographic orientation of the dendritic cells with respect

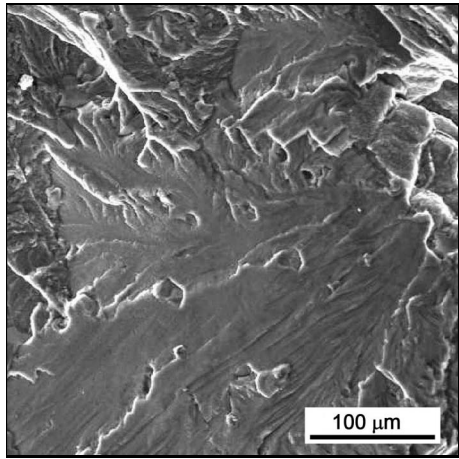


Fig. 10. Fatigue fracture facet with river pattern (region B).

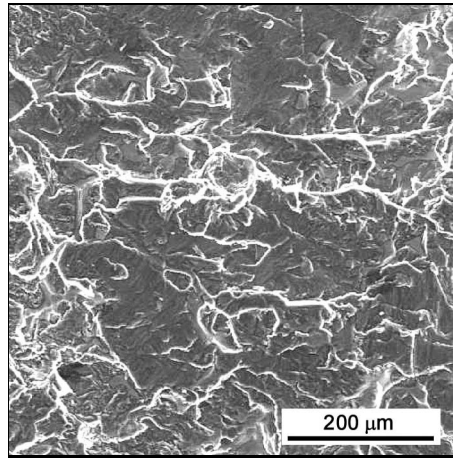


Fig. 11. Morphology of fracture surface from region C.

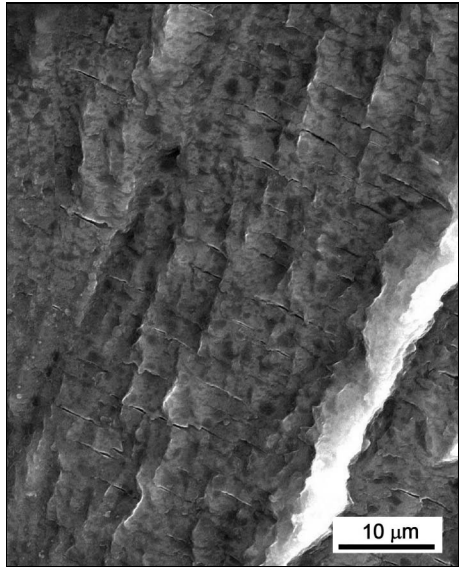


Fig. 12. Detail view on region C. Fracture facets with network of parallel microcrack.

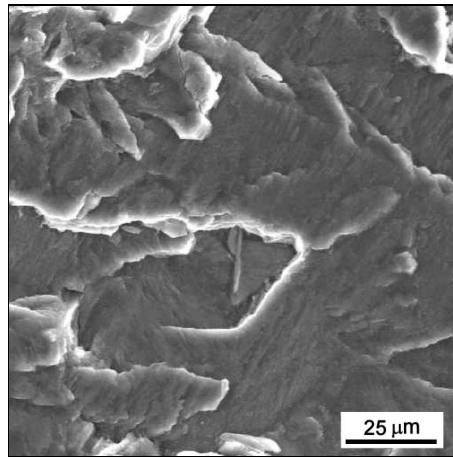


Fig. 13. Tiny, not very marked, fatigue striations on fracture surface in region C.

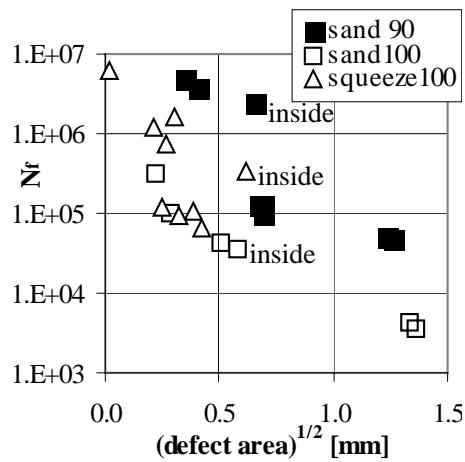


Fig. 14. Dependence of lifetime N_f on the initiation defect area square rooted.

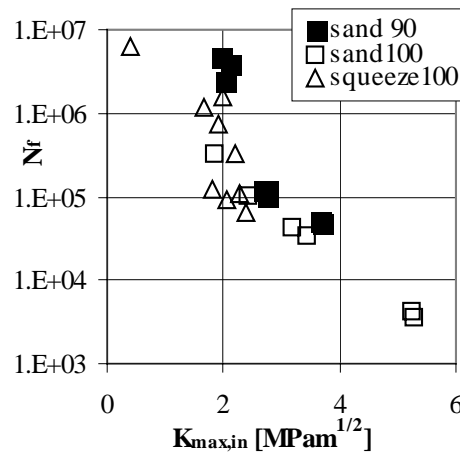


Fig. 15. Dependence of lifetime N_f on the maximum stress intensity factor $K_{\max,\text{in}}$ in the tip of the initiation defect.

to the stress direction and to the local fatigue crack propagation direction. A network of parallel microcracks is observed on many fatigue patches (Fig. 12) and tiny, not very marked fatigue striations are seen in some areas (Fig. 13).

The mechanism of failure described above pass into the final fracture, characterized by interdendritic failure with a clearly rugged surface topography. Owing to the appreciable difference between the nature of region C, failed by the fatigue mechanism, and the final fracture surface (region D), it is rather easy to distinguish between these parts of the fracture surface plane and to determine the total length l_u and area of the fatigue fracture A_u . The values were nearly identical in all samples, $l_u = (2.3 \pm 0.1)$ mm and $A_u = (7.7 \pm 0.7)$ mm² at the stress level 90 MPa and $l_u = (1.8 \pm 0.3)$ mm and $A_u = (5.4 \pm 0.6)$ mm² at the stress level 100 MPa.

Fatigue crack initiation was studied also quantitatively. Figure 4 shows the regions with pores, whose projected sections A_{def} were measured and used in the definition of the critical distance for defect sorting (see section 2). The area of defects, along with the corresponding square roots, the maximum initiation stress intensity factor $K_{\max,\text{in}}$, and number of cycles to fracture N_f , are given in Table 3. In Fig. 14, the lifetimes N_f are plotted as a function of defect area square root $A_{\text{def}}^{1/2}$. The correlation between lifetime N_f and maximum initiation stress intensity factor $K_{\max,\text{in}}$, calculated according to Eq. (1), is plotted in Fig. 15.

Table 3. Quantitative parameters of initiation defects in AZ91 alloy prepared by sand casting

Sample	Load (max. stress) [MPa]	Defect area [mm ²]	(Defect area) ^{1/2} [mm]	$K_{\max, \text{in}}$ [MPa · m ^{1/2}]	Fatigue crack length [mm]	Fatigue area [mm ²]	N_f	Type of defect
1	90	0.123	0.351	1.94	2.3	8.2	4780000	outside
2		0.427	0.653	2.04	2.3	7.9	2550000	inside
3		0.163	0.404	2.08	2.2	7.5	3880000	outside
4		0.456	0.675	2.69	2.0	6.2	125000	outside
5		0.480	0.693	2.73	2.2	8.1	124000	outside
6		0.481	0.694	2.73	2.5	8.6	103000	outside
7		1.513	1.230	3.64	2.5	8.7	52000	outside
8		1.590	1.261	3.68	2.1	6.7	49000	outside
b1	100	2.041	1.429	5.40	1.6	4.8	4200	outside
b2		0.332	0.576	3.43	1.8	5.0	35000	outside
b3		0.084	0.289	2.43	1.7	5.9	102000	outside
b4		0.210	0.459	3.06	1.6	5.1	42000	outside
b5		0.045	0.211	1.82	2.3	6.6	405000	inside
b6		0.048	0.220	2.12	2.1	5.2	325000	outside

b) AZ91 samples prepared by squeeze casting

In the samples issued from squeeze casting, fatigue cracks initiated mostly from structure defects on specimen surface or immediately beneath the surface. Internal defects acted as initiation sites only in two samples. The structure defects that served as the initiation centres can be divided into 4 groups:

a) Thin continuous film (Fig. 16). Energy dispersive X-ray analysis revealed that the film mostly consists of manganese. Apart from the slightly higher Al and Zn contents, no other elements were observed. Isolated tiny particles were observed on film surface and also contained mainly manganese.

b) Cluster of tiny particles. Energy dispersive X-ray analysis revealed the presence of Ca in this area.

c) Zone with a cluster of pores. This type of defect was observed in one case, where tiny Ca-containing particles were present at the pore site.

d) Isolated coarse particle. A coarse particle, 23.5 μm in diameter, acted as initiation centre in one case.

The results of the quantitative evaluation of the area of defects serving as centres of fatigue crack initiation in the samples issued for squeeze casting, along with defect area square roots, $K_{\max, \text{in}}$, and N_f , are given in Table 4. The correlations

Fig. 16. Thin continuous film that acted as initiation sites of fatigue crack of AZ91 sample prepared by squeeze casting.

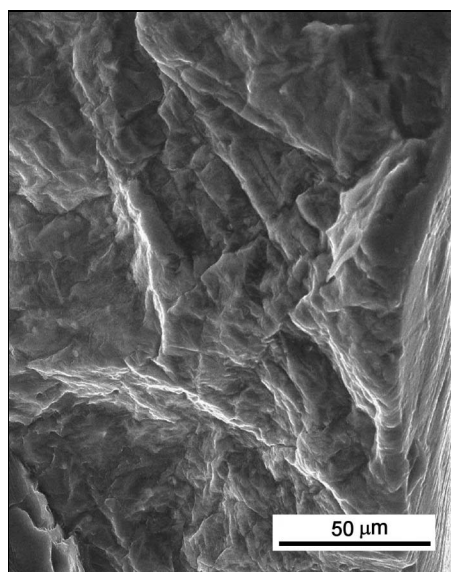


Table 4. Quantitative parameters of initiation defects in AZ91 alloy prepared by squeeze casting

Sample	Defect area [mm ²]	(Defect area) ^{1/2} [mm]	$K_{\max, \text{in}}$ [MPa·m ^{1/2}]	Fatigue crack length [mm]	Fatigue area [mm ²]	N_f	Type of defect
2	0.3790	0.62	2.19	2.40	4.82	326600	inside
3	0.0880	0.30	1.98	1.90	5.26	1592000	outside
4	0.0750	0.27	1.91	1.90	5.45	741000	outside
5	0.1490	0.39	2.26	2.10	7.03	109300	outside
6	0.1010	0.32	2.05	2.20	6.84	93500	outside
7	0.0004	0.02	0.41	1.60	4.48	6139700	inside
8	0.0610	0.25	1.81	1.80	5.34	122500	outside
9	0.0430	0.21	1.66	1.80	5.76	1190700	outside
10	0.1810	0.42	2.37	1.80	4.90	64300	outside

between N_f and $A_{\text{def}}^{1/2}$ or $K_{\max, \text{in}}$ are plotted in Figs. 14 and 15.

From the qualitative point of view, the mechanism of fatigue crack propagation was the same as in the sand-cast alloy, except for region A, which was never found in squeeze cast samples. All fatigue cracks in squeeze-cast samples were roughly of the same size, i.e. of length $l_u = (1.9 \pm 0.2)$ mm and area $A_u = (5.5 \pm 0.7)$ mm².

4. Discussion

The total fatigue life N_f of test specimens is the sum of the number of cycles needed for the initiation of cracks and the number of cycles needed for the growth of cracks to their critical length (or area) at which a fast final fracture takes place. Both stages of fatigue life are affected by microstructure parameters, namely: a) the volume fraction of pores, their dispersion and distribution throughout the sample; b) the presence of other structure defects, such as impurities in the form of film, clusters of tiny particles, or larger isolated inclusions; c) the size of dendritic cells and interdendritic β -phase particles. The individual effects of various structure parameters on both fatigue life stages and the total fatigue lifetime can have different weights.

In the alloy prepared by sand casting, the fatigue cracks invariably initiate from pores. The results of the quantitative evaluation presented in Table 3 and Fig. 14 demonstrate that the total lifetime N_f decreases appreciably with increasing size of the pores from which the crack has initiated (represented here by the square root of defect projection area). Given a constant pore area, a defect located at test specimen surface exerts a larger effect than a defect located inside (Fig. 14). Some authors [8, 13] relate the effect of pore area on fatigue crack initiation on the base of linear fracture mechanics principles. Murakami and Endo [13] suggest that the stress intensity factor acting at the tip of the defect depends primarily on the area and location of the defect, while the effect of pore shape is of minor importance [14, 15, 16]. Based on those premises, the authors of [13] derived Eq. (1) for calculation of the maximum stress intensity factor for cycle asymmetry $R = -1$. The correlation of the total lifetime N_f and the maximum stress intensity factor $K_{\max, \text{in}}$, calculated according to Eq. (1), is plotted in Fig. 15. The plot demonstrates that there is a strong dependence of N_f on the maximum stress intensity factor $K_{\max, \text{in}}$ also in our case, particularly for defects consisting in pores in the alloy prepared by sand casting.

In all samples prepared by sand casting loaded at the same stress level, the values of the total fatigue length l_u and area A_u are roughly the same ($l_u = (2.3 \pm 0.1)$ mm, $A_u = (7.7 \pm 0.7)$ mm² at 90 MPa and $l_u = (1.8 \pm 0.3)$ mm, $A_u = (5.4 \pm 0.6)$ mm² at 100 MPa) and no differences are observed in crack growth mechanisms and their occurrence on the fracture surface. Therefore, it is reasonable to assume that there is not an appreciable difference among the samples in crack propagation period and the lifetime within this period for the same stress level. The large scatter of total lifetime N_f is probably primarily due to the different magnitude of initiation defects of pore type and its effect on the time necessary for fatigue crack initiation and the early stage of its propagation.

The above observations are consistent with published data for magnesium alloys [8, 17, 18, 19] and aluminium alloys [8, 20, 21]. The size of the defects and

their location near the surface of fatigue samples play a major role in affecting the total fatigue lifetime. Large near-surface defects induce higher stress concentration and accelerate the initiation of fatigue cracks [16, 18]. Large defects also bring about formation of larger starting cracks. Such cracks are then acted upon by a larger driving force. In other words, a higher stress intensity factor acts on their tips, bringing about a faster initial crack growth. This hypothesis is supported by an in situ observation of the nucleation and initial propagation of fatigue cracks in AM60B magnesium alloy obtained by high-pressure die casting. In the materials with larger pores the cracks initiate markedly sooner than in those with smaller pores, or than those initiated in persistent slip band inside of larger dendrites [17].

Higher total porosity (volume fraction of pores) is connected with higher probability of occurrence of pores near the sample surface, affecting adversely the fatigue lifetime. However, according to [18, 20], this effect is of secondary importance. The total lifetime during high-cycle fatigue exhibits no strong correlation with pore density, instead, it rather correlates with the maximum size of the pores that serve as fatigue-crack initiation centres [18]. Other microstructure parameters, such as particles, dendrite size, or grain size, are also of minor importance with respect to the lifetime [18, 21].

Although containing virtually no pore type defects, the samples prepared from squeeze-cast material also exhibit large scatter of the total lifetimes N_f . Fractographical observations revealed that in those samples, also, fatigue cracks initiate from structure defects. Quantitative evaluation revealed similar dependences of lifetime N_f on the defect size A_{def} or on the maximum stress intensity factor $K_{\text{max,in}}$ (Figs. 14, 15). The larger scatter of the experimental points as compared to the analogous dependences for the sand-cast samples may be due to the presence of different defect types in the samples (film, clusters of inclusions or isolated coarse particles).

Although the final fracture of samples produced by squeeze casting occurred at a shorter fatigue crack length (smaller fatigue crack area), the mean total lifetime was the same as for the samples produced by sand casting, despite the different stress levels applied (100 MPa for squeeze casting and 90 MPa for sand casting). At stress level of 100 MPa, the mean fatigue life (50% probability of fracture) of the squeeze cast material is higher than this of sand cast material in spite of the fact that the length of fatigue cracks in both is approximately the same. The better mean lifetime for a 50% probability to failure of the alloy prepared by squeeze casting may be due either to a less unfavourable effect of structure defects on fatigue crack initiation or, also, to a higher resistance against fatigue crack growth. In view of the probably smaller effect of dendrite size on fatigue lifetime [18, 21], a rather marked effect on the initiation stage and initial crack growth can be assumed. This assumption, however, needs to be proved by experiments initiation period and early

stage of crack growth aimed at determining the growth rate in both alloys: sand- and squeeze-cast.

From the qualitative point of view, the fatigue failure mechanisms were similar for both casting processes. The fatigue fracture surfaces exhibited two or, rarely, three morphologically different regions (labelled A, B, C in the figure). Region B, closer to the initiation site, was characterized by a microscopically rough surface, formed by serrated facets or by smoother facets with river-like patterns. The orientation of the serrations (steps) was appreciably different in the individual facets. The shape of the fracture line in the region labelled B (Fig. 6) indicates that the fracture process is mostly transcrystalline here. Local interdendritic fracture, if any, is associated with the occurrence of fine pores on the boundaries of the dendrites (Fig. 6). In situ observation of the failure of AM60B cast Mg alloy on a scanning microscope [17] gives evidence that the transcrystalline propagation of short cracks proceeds in slip bands and may include plastic deformation in the neighbouring grains. In view of this we suggest that the observed transcrystalline failure within the region B takes place through plastic deformation mechanisms, i.e. dislocation generation and motion in a limited number of slip planes, that are mechanisms reported for hexagonal structure alloys, e.g. in [22, 23].

The subsequent crack propagation in region C is transcrystalline, with a fatigue fracture surface morphology consisting of microareas (patches) separated by microsteps. Despite of the fact that somewhat more complex patterns are observed, this morphology is similar to fatigue fracture surface resulting from mechanism of striation formation. Locally, hints of striations, or of parallel secondary cracks, were actually found.

Note that the fatigue crack propagation observed in this work differs rather markedly from the mechanisms of failure of the AZ91E-T4 die-cast magnesium alloy reported in [18]. The authors of this paper have observed near to the initiation site a smooth surface of transcrystalline fracture covered by fine fatigue striations and affecting an area of a large number of dendritic cells. At low magnification this smooth area is similar to zone A in the samples presented here, which was observed only occasionally. However, a detailed view at high magnification gives evidence that the fine morphology, and hence the process of its formation, is entirely different (Fig. 8). By its morphology, the fracture area adjacent to the smooth surface with fine striations reminds of zone B, although the authors [18] suggest an interdendritic propagation patterns for it. No fracture surface area with a morphology approaching our region C was observed in [18].

5. Conclusions

The following conclusions are drawn from the structure analyses, mechanical and fatigue testing of AZ91 alloy samples prepared by two different casting procedures and without any additional heat treatment:

1. The alloys contain a massive $Mg_{17}Al_{12}$ phase at dendrite boundaries and lamellar precipitates of this phase. The structure of the samples prepared by squeeze casting contains finer grains than the samples prepared by sand casting, with a tinier form of occurrence of both the massive $Mg_{17}Al_{12}$ phase and its precipitates.

2. Casting defects (pores), which are observed in the alloy prepared by sand casting, are virtually absent from the samples prepared by squeeze casting. The latter samples, however, exhibit oxide film, clusters of tiny particles or isolated coarse particles.

3. The sand-cast material exhibits shorter fatigue life as compared to the squeeze-cast material. At stress level of 100 MPa, the mean fatigue life determined for 50% probability to failure is of 3.9×10^4 and 3.3×10^5 cycles for the sand-cast and squeeze-cast material, respectively. Fatigue life of the same magnitude, i.e., of 3.3×10^5 cycles, as this exhibited by the squeeze-cast material, is measured in the sand-cast material at stress level of 90 MPa, i.e., at stress level of 10 % lower than this sustained by the squeeze cast material.

4. In the alloy prepared by sand casting, the high data scatter of lifetimes N_f is due to the presence of large pores. Although the squeeze casting process eliminates the porosity and improves the fatigue life, the structure defects present once again are the cause of a large scatter of lifetime values.

Acknowledgements

The results reported in the present paper were obtained within Project 106/03/0903 with the financial support from the Czech Science Foundation.

REFERENCES

- [1] DAS, S.: JOM, 2003, 55, p. 22.
- [2] POWELL, B. R.: JOM, 55, 2003, p. 28.
- [3] AGHION, E.: JOM, 55, 2003, p. 30.
- [4] BARIL, E.: JOM, 55, 2003, p. 34.
- [5] BAKKE, P.—PETTERSEN, K.—WESTENGEN, H.: JOM, 55, 2003, p. 46.
- [6] LAMARK, T. T.—CHMELÍK, F.—ESTRIN, Y.—LUKÁČ, P.: Kovove Mater., 42, 2004, 5, p. 293.
- [7] OZTURK, K.—ZHONG, Z.—LUO, A. A.: JOM, 55, 2003, p. 40.
- [8] MAYER, H.: Int. Journal of Fatigue, 25, 2003, p. 245.
- [9] OGAREVIC, V. V.—STEPHENS, R. I.: Annu. Rev. Mater. Sci., 20, 1990, p. 141.
- [10] SMOLA, B.: Z. Metallkunde, 94, 2003, p. 5.
- [11] SMOLA, B.: Phys. Stat. Sol. (a), 1, 2002, p. 305.
- [12] OČENÁŠEK, V.—HNILICA, F.: In: Proceed. of the 13th Internat. Metallurgical and Materials Conf. METAL 2004. [CD-ROM]. Ostrava, TANGER Ltd., no. 145.
- [13] MURAKAMI, Y.—ENDO, M.: In: Proc. Theoretical Concepts and Numerical Analysis of Fatigue, Birmingham, UK. Warley: Engineering Materials Advisory Services Ltd., Cradley Heath 1992, p. 51.
- [14] MURAKAMI, Y.: Stress Intensity Factors Handbook. Vol. 1. Oxford, Pergamon Press 1987.

-
- [15] MURAKAMI, Y.: *Eng. Fract. Mech.*, 22, 1985, p. 101.
- [16] GALL, K.—HORSTEMEYER, M. F.—DEGNER, B. W.—McDOWELL, D.—FAN, J.: *Int. J. Fract.*, 108, 2001, p. 207.
- [17] GALL, K.—BIALLAS, G.—MAIER, H. J.—GULLET, P.—HORSTEMEYER, M. F.—McDOWELL, D. L.—FAN, J.: *Int. Journal of Fatigue*, 26, 2004, p. 59.
- [18] HORSTEMEYER, M. F.—ZANG, N.—McDOWELL, D. L.—FAN, J.—GULLET, P. M.: *Acta Materialia*, 52, 2004, p. 1327.
- [19] HÖPPEL, H. W.—EISENMEIER, G.—HOLZWARTH, B.—MUGHRABI, H.: In: *Magnesium Alloy and their Applications*, Munich 2000. Ed.: Kainer, K.U. Weinheim, Wiley-VCH 2000, p. 348.
- [20] YI, J. Z.—GAO, Y. X.—LEE, P. D.—FLOWER, H. M.—LINDLEY, T. C.: *Met. Trans.*, 34A, 2003, p. 1879.
- [21] BOILEAU, J.—ALLISON, J. E.: *Met. Trans.*, 34A, 2003, p. 1807.
- [22] BEEVERS, C. J.: *Metal Science*, 1980, p. 418.
- [23] BACHE, M. R.: *Int. Journal of Fatigue*, 21, 1999, p. 2105.